Tightly-Twisted One-Handed Helical Tubular Ladder Polymers with π-Electron-Rich Cylindrical Helical Cavities for Chromatographic Enantioseparation

Wei Zheng,[a] Kosuke Oki,[a] Ranajit Saha,[b] Yuh Hijikata,[b] Eiji Yashima,*[a] and Tomoyuki Ikai*[a],[c]

[a] Dr. W. Zheng, Dr. K. Oki, Prof. E. Yashima, Dr. T. Ikai
Department of Molecular and Macromolecular Chemistry
Graduate School of Engineering, Nagoya University
Chikusa-ku, Nagoya 464-8603 (Japan)
E-mail: yashima@chembio.nagoya-u.ac.jp; ikai@chembio.nagoya-u.ac.jp

[b] Dr. R. Saha, Dr. Y. Hijikata
Institute for Chemical Reaction Design and Discovery (WPI-ICReDD)
Hokkaido University
Sapporo 001-0021 (Japan)

[c] Dr. T. Ikai
Precursory Research for Embryonic Science and Technology (PRESTO)
Japan Science and Technology Agency (JST)
Kawaguchi, Saitama 332-0012 (Japan)

Supporting information for this article is given via a link at the end of the document.

Abstract: Defect-free one-handed contracted helical tubular ladder polymers with a π-electron-rich cylindrical helical cavity were synthesized by alkyne benzannulations of the random-coil precursor polymers containing 6,6´-linked-1,1´-spirobiindane-7,7´-diol-based chiral monomer units. The resulting tightly-twisted helical tubular ladder polymers showed remarkably high enantioseparation abilities toward a variety of chiral hydrophobic aromatics with point, axial, and planar chiralities. The random-coil precursor polymer and analogous rigid-rod extended helical ribbon-like ladder polymer with no internal helical cavity exhibited no resolution abilities. The molecular dynamics simulations suggested that the π-electron-rich cylindrical helical cavity formed in the tightly-twisted tubular helical ladder structures is of key importance for producing the highly-enantioseparation ability, by which chiral aromatics can be enantioselectively encapsulated by specific π–π and/or hydrophobic interactions.

Introduction

Biological macromolecules, such as left (*M*)-handed helical amylose[1] and right (*P*)-handed triple-stranded helical schizophyllan and curdlan[2] as well as assembled proteins,[3] are known to possess an intrinsic nanoscale chiral cavity or pore. Hence, such biomacromolecules form supramolecular inclusion complexes with a variety of guest molecules and polymers through specific encapsulation within the hydrophobic cavities in water driven by hydrophobic interactions, which contribute greatly to their specific functionalities related to catalysis, recognition, and transport.[4] Taking inspiration from these helical host systems in nature, a number of artificial helical foldamers[5] and polymers,[6] such as syndiotactic poly(methyl methacrylate) (st-PMMA),[7] has been developed. These foldamers and st-PMMA fold into preferred-handed helices with a unique helical cavity, thus forming inclusion complexes with target molecules and polymers in a highly molecular- and/or enantio-selective manner.[5b,8] However, such helical cavities are mostly dynamic, hence, guest molecules are encapsulated by an induced-fit mechanism, resulting in limited applications as chiral materials, particularly, for separating enantiomers[8e,h] and asymmetric catalysis.[5c,9]

Since the first synthesis of ladder-like polymers by Deusen in 1966,[10] a class of unique shape-persistent ladder polymers consisting of conformationally restricted rigid repeating units has been of increasing interest due to their intriguing physical and mechanical properties along with outstanding chemical and thermal stabilities, which are inaccessible from the traditional polymers consisting of a single bond between the monomer units.[11] We previously reported the first optically-active ladder polymers with a one-handed helical geometry[12] through an acid-promoted alkyne benzannulation developed by Goldfinger and Swager.[13] The resulting one-handed helical ladder polymers composed of an enantiopure bulky triptycene framework possess a rigid helical ladder structure and partially separated some racemic compounds into enantiomers when applied as a chiral stationary phase (CSP) for high-performance liquid chromatography (HPLC). However, its resolving ability was poor probably due to the lack of a concave helical cavity suitable for interactions with enantiomers.[12] The acid-promoted alkyne benzannulation has not always provided completely defect-free conjugated ladder polymers and polycyclic aromatics due to unavoidable side reactions including the formation of spiro linkages[14] and rearrangements of aryl pendants[15] because of highly-reactive vinyl cation intermediates, thus producing a complicated product mixture. To overcome such a drawback, we have recently found that the introduction of 2,6-dimethyl substituents on the 4-alkoxyphenylethynyl pendants of the precursor polymers completely suppresses any undesired reaction pathways during the acid-promoted alkyne benzannulations,[15b] thus producing the defect-free one-handed helical spiro-conjugated ladder polymers with an intense

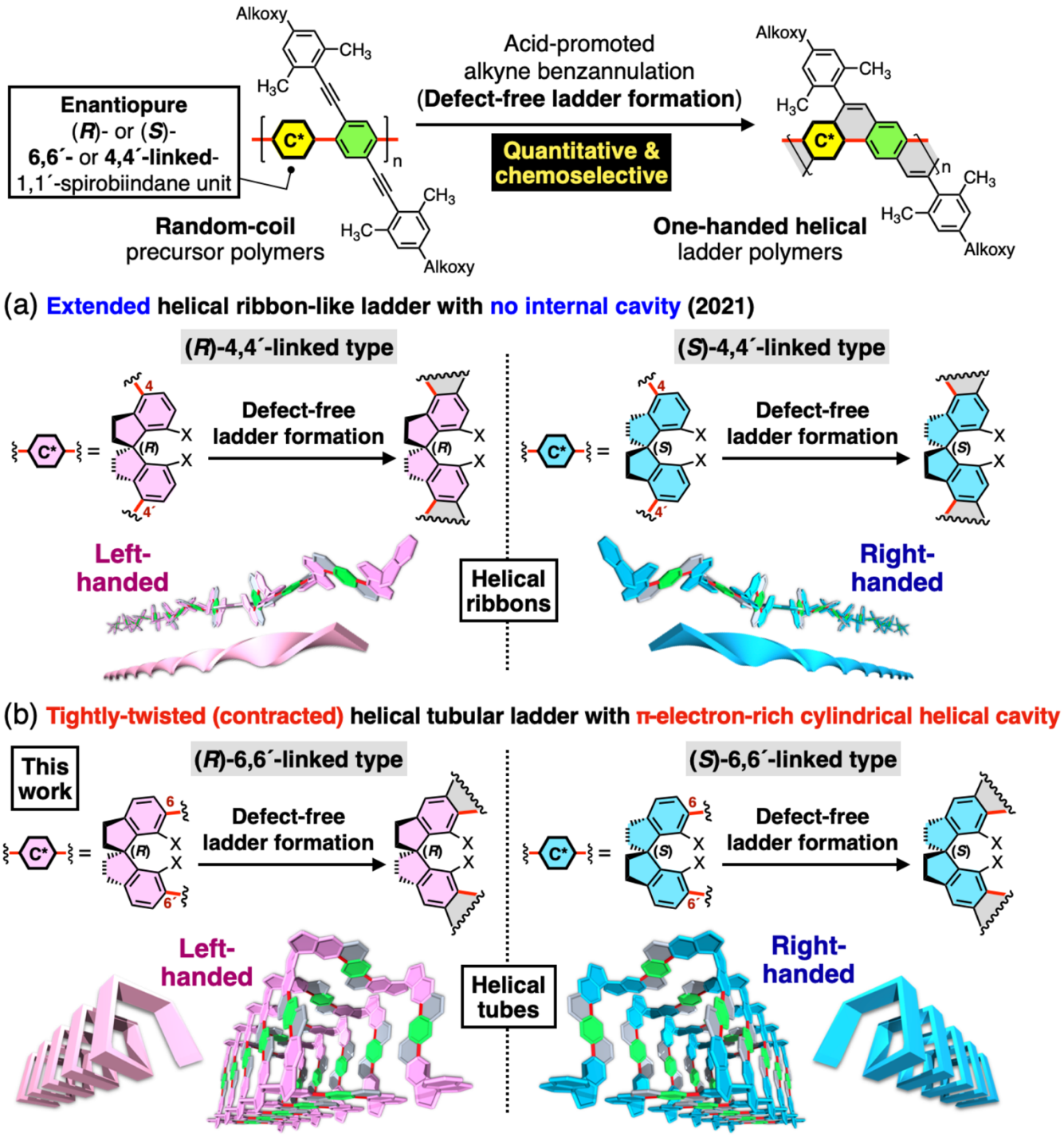

Figure 1. (a,b) Schematic illustrations of rationally designed synthesis of left (*M*)- and right (*P*)-handed extended ribbon-like (a) and tightly-twisted (contracted) tubular (b) helical ladder polymers through quantitative and chemoselective acid-promoted alkyne benzannulations of the corresponding random-coil precursor polymers containing an enantiopure 1,1´-spirobiindane unit with a different linkage position (4,4´- or 6,6´-linkage, respectively). The extended ribbon-like helical ladder polymers have no internal helical cavity (a), while the contracted tubular helical ladder polymers possess a π-electron-rich cylindrical helical cavity (b).

circularly polarized luminescence (CPL) (Figure 1a). Based on this strategy, we have also successfully synthesized coplanar fully π-conjugated ladder polymers[15b] and consecutively-fused multiple expanded helicenes[16] in a quantitative and perfect chemoselective manner. The one-handed helical spiro-conjugated ladder polymers have a rigid, but extended helical ribbon-like ladder structure with no internal cavity (Figure 1a).[15b] The synthesis of optically-active helical ladder polymers containing spirobifluorene frameworks as chiral sources with and/or without a helical cavity has also been reported by Takata et al.[17] and recently by Meskers et al.,[18] but their structural

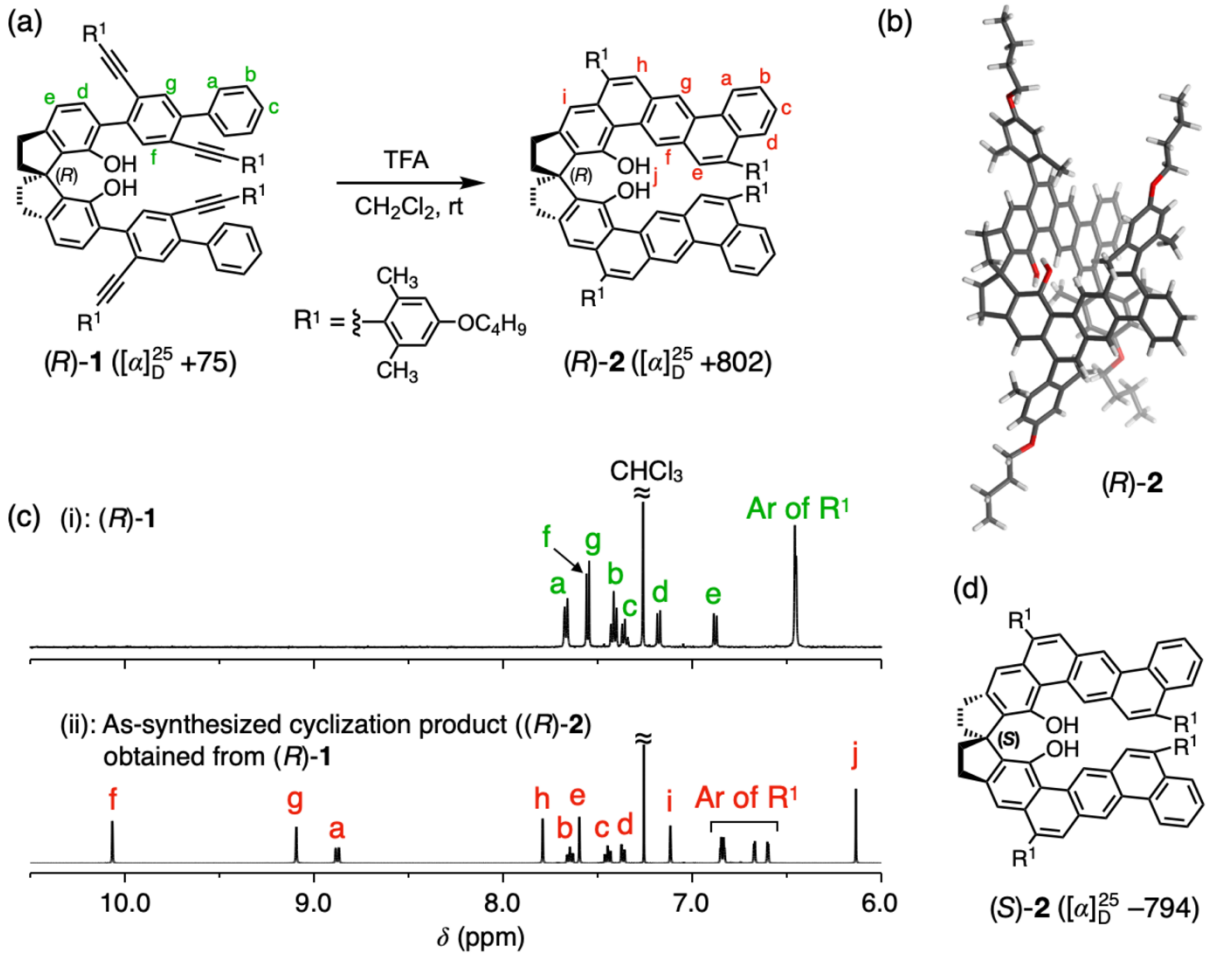

Figure 2. (a) Synthesis of an optically-active spiro-conjugated ladder-type molecule ((*R*)-**2**) through acid-promoted alkyne benzannulation of (*R*)-**1**. (b) X-ray crystal structure of (*R*)-**2**. (c) ^{1}H NMR spectra (500 MHz, $CDCl_3$, 25 °C) of (*R*)-**1** (i) and an as-synthesized cyclization product obtained from (*R*)-**1** (ii). For the signal assignments and the corresponding IR spectra, see Figures S7–S9. (d) Structure of (*S*)-**2**.

integrities were not completely elucidated.

Taking advantage of the structural designability and integrity of helical ladder polymers due to their rigid and robust three-dimensional helical framework derived from an exceptionally restricted conformational freedom,[12,15b] we envisioned that one-handed helical ladder polymers with a discrete π-electron-rich tubular helical cavity together with a controlled helix-sense and helical pitch suitable for recognizing enantiomers within the helical cavities could be precisely synthesized by a rational design of the precursor polymers. To this end, we designed novel precursor polymers composed of alternating enantiopure (*R*)- or (*S*)-6,6´-linked-1,1´-spirobiindane-7,7´-diol (6,6´-SPINOL) and achiral 2,5-bis[2-(4-alkoxy-2,6-dimethylphenyl)ethynyl]-1,4-phenylene units, which are different from the previously reported precursor polymers[15b] in the linkage positions of the spirobiindane segments (Figure 1a,b). Thus, we expected that the newly-synthesized random-coil precursor polymers would be quantitatively and chemoselectively converted into the contracted one-handed helical spiro-conjugated tubular ladder polymers possessing a unique π-electron-rich cylindrical helical cavity through the modified acid-promoted alkyne benzannulations that we have developed (Figure 1b).[15b] The primary and secondary structures of the resulting contracted one-handed helical tubular ladder polymers and emergence of a high enantioseparation ability when used as a CSP for HPLC due to its unique π-electron-rich cylindrical helical cavity are reported (Figure 1b). A plausible mechanism for the chiral recognition in the π-electron-rich tubular helical cavity was also proposed based on the dynamics of the contracted and extended helical ladder polymers with tubular and ribbon geometries, respectively, obtained from molecular dynamics (MD) simulations.

Results and Discussion

Defect-Free Synthesis of Tightly-Twisted One-Handed Helical Tubular Ladder Polymers

First, 6,6´-SPINOL-based cyclization model precursors ((*R*)- and (*S*)-**1**) with four 2-(4-butoxy-2,6-dimethylphenyl)ethynyl pendants were synthesized, then subjected to trifluoroacetic acid (TFA)-promoted intramolecular alkyne benzannulations according to our previously reported procedure (Figures 2a and S1).[15b] The four-fold intramolecular cyclizations of (*R*)- and (*S*)-**1** quantitatively and

Table 1. Copolymerization results of Ph-B_2 with (*R*)- and (*S*)-6,6´-SPR and (*R*)- and (*S*)-4,4´-SPR using P(*t*-Bu)$_3$ Pd G2 in the presence of K_3PO_4 in THF/H_2O (2/1, v/v) at room temperature for 12 h[a]

Entry	Monomer in feed (mol%)		Copolymer				
			Sample code	Yield (%)	M_n (10^4)[b]	M_w/M_n [b]	DP_n [c]
1	(*R*)-6,6´-SPR (50)	Ph-B_2 (50)	poly-**3R**	69	1.34	1.40	15
2	(*S*)-6,6´-SPR (50)	Ph-B_2 (50)	poly-**3S**	68	1.36	1.41	16
3	(*R*)-4,4´-SPR (50)	Ph-B_2 (50)	poly-**5R**	72	1.15	1.25	13
4	(*S*)-4,4´-SPR (50)	Ph-B_2 (50)	poly-**5S**	75	1.12	1.23	13

[a] [SPR] = [Ph-B_2] = 0.33 M, [P(*t*-Bu)$_3$ Pd G2] = 17 mM, [P(*t*-Bu)$_3$ Pd G2]/[K_3PO_4] = 1/120. [b] Estimated by SEC (polystyrene standards) with chloroform as the eluent. [c] Number-average degree of polymerization estimated by M_n.

chemoselectively proceeded, thus affording (*R*)- and (*S*)-**2**, respectively, in >99% NMR yields (Figures 2a,c,d and S1), as a result of defect-free annulative π-extensions without any byproducts, as confirmed by their well-assigned ^{1}H NMR signals and IR analyses (Figures 2c and S7a–d). The spiro-conjugated ladder structure of (*R*)-**2** was unambiguously determined by single-crystal X-ray crystallography (Figures 2b and S5) and further supported by their 2D NMR (Figure S9) and high-resolution atmospheric pressure chemical ionization mass spectra (APCI-MS) analyses (Section 2 in the Supporting Information).

With the above successful results of the defect-free synthesis of the unimer models ((*R*)- and (*S*)-**2**) in hand, we then synthesized contracted one-handed helical tubular ladder polymers with a cylindrical helical cavity through the acid-promoted intramolecular alkyne benzannulations of the precursor polymers (poly-**3R** and poly-**3S**) (Figures 3a, S2, and S3). Poly-**3R** and poly-**3S** were designed and synthesized by the Suzuki–Miyaura coupling copolymerization of Ph-B_2 with 6,6´-dibromo derivatives of (*R*)- and (*S*)-6,6´-SPINOL ((*R*)- and (*S*)-6,6´-SPR, respectively) (Figures 3a and S2). The number-average molar masses (M_n) of the obtained poly-**3R** and poly-**3S** were estimated to be 1.34×10^4 and 1.36×10^4, respectively, by size-exclusion chromatography (SEC), corresponding to the degree of polymerization (DP) of 15–16 (entries 1 and 2 in Table 1). Poly-**3R** and poly-**3S** were then treated with TFA to transform their backbone structures from random-coil to one-handed helical tubular ladder structures (Figures 3a and S3). After a 12-h reaction, the alkyne groups in poly-**3R** and poly-**3S** were completely consumed, as supported by IR analysis (Figure S7e–h). The M_n values of poly-**4R** and poly-**4S** (ca. 1.30×10^4) were almost the same as those of the random-coil precursors, poly-**3R** and poly-**3S** (ca. 1.35×10^4) (Figures 3a,c and S3). The matrix-assisted laser desorption-ionization time-of-flight mass (MALDI-TOF-MS) spectrum of poly-**4R** displayed a main series of peaks with a regular interval of approximately 866.5 (*m*/*z*) mass that corresponds to the molar mass of the repeating unit (Figure S12b). Poly-**4R** also showed a simple single set of ^{1}H NMR signals including three aromatic proton resonances due to its regular spiro-conjugated ladder backbone (Figure 3b(ii)), which could be unequivocally assigned by 2D NMR analysis (Figure S11). All of these data support the defect-free spiro-conjugated ladder polymer formation that took place in a complete chemoselective manner as expected from the model reaction results (Figure 2). For comparison, the rigid-rod (*M*)- and (*P*)-handed extended helical spiro-conjugated ribbon-like ladder polymers (poly-**6R** and poly-**6S** in Figure 3d) bearing hydroxy groups instead of ethoxy ones at the chiral 1,1´-spirobiindane segments with no helical cavity[15b] were also prepared from their poly-**5R** and poly-**5S** precursors according to the previously reported procedure (Table 1 (entries 3 and 4) and Figures S2 and S3).[15b]

Chiroptical Enhancement through Helical Ladderization

The precursor polymers (poly-**3R** and poly-**3S**) exhibited negligibly weak circular dichroism (CD) and CPL responses, which were dramatically enhanced after helical ladderization. Thus, poly-**4R** and poly-**4S** showed intense mirror-imaged CD and clear CPL signals (Figure 3e,f) as observed for poly-**6R** and poly-**6S** (Figure S13c,d). Concurrently, the optical rotation values of the contracted tubular helical poly-**4R** and poly-**4S** ($[\alpha]_D^{25}$ = +942 and –931) increased almost eightfold as compared to those of the precursors ($[\alpha]_D^{25}$ = +122 and –119), which were significantly higher than those of the extended ribbon-like helical poly-**6R** and poly-**6S** ($[\alpha]_D^{25}$ = +267 and –253) (Figure 3a,c,d). A similar enhancement of the CD and CPL intensities and optical rotation before and after the helically-twisted ladder formation was also observed for the unimer models of (*R*)- and (*S*)-**2** (Figures 2a and S14). On the other hand, the CD and photoluminescence (PL) spectral patterns of poly-**4R** were quite different from those of poly-**6R**, particularly in their long absorption regions (Figures 3e,f and S13c,d). The observed differences in their chiroptical and PL properties between poly-**4R**/poly-**4S** and poly-**6R**/poly-**6S** are most likely due to the difference in their helical structures, i.e., contracted tubular and extended ribbon-like helical ladder structures derived from the different 6,6´- and 4,4´-linkage

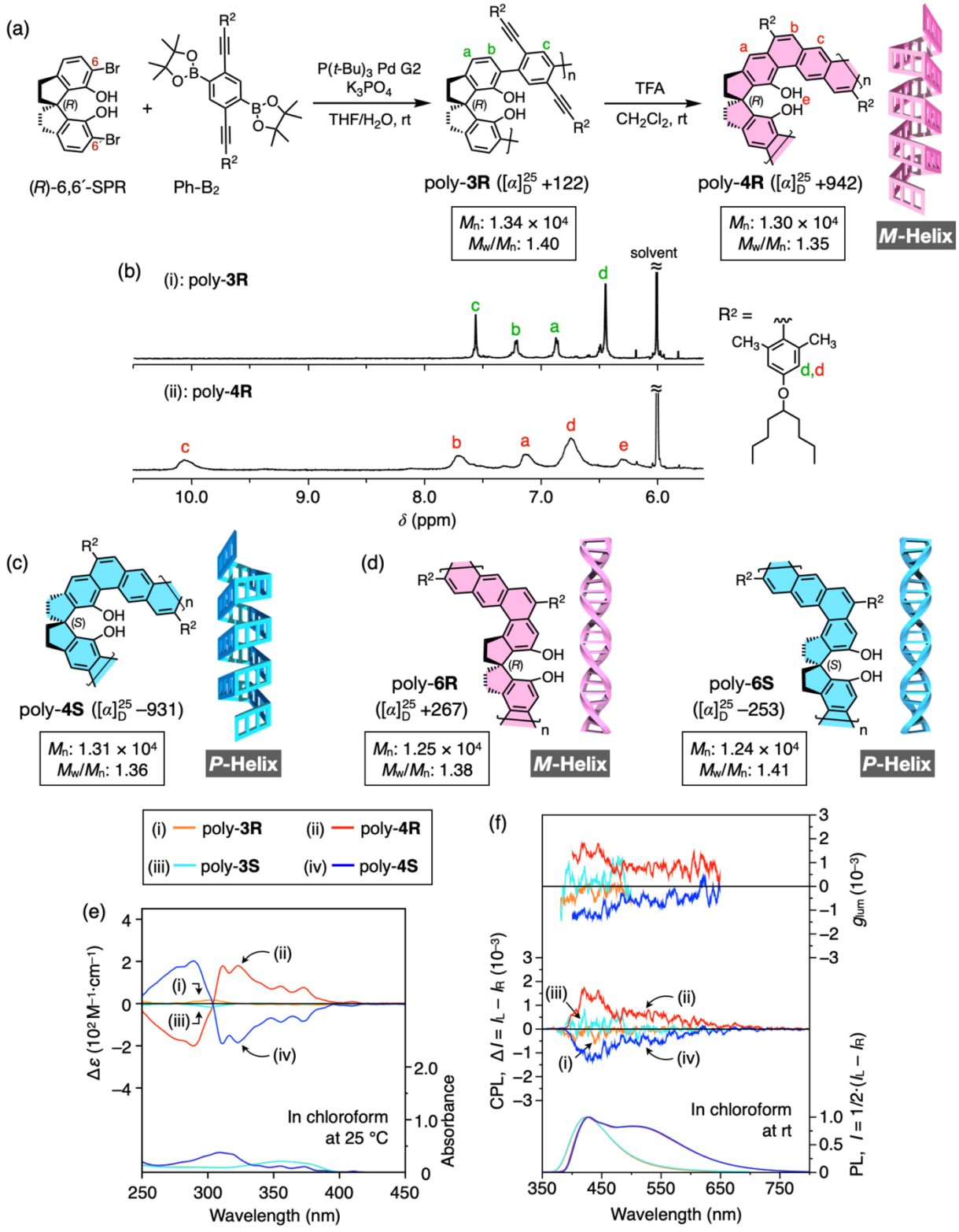

Figure 3. (a) Synthesis of (*M*)-handed helical tubular ladder polymer (poly-**4R**) through Suzuki–Miyaura coupling copolymerization of (*R*)-6,6′-SPR and Ph-B_2, followed by quantitative and chemoselective cyclizations of poly-**3R**. (b) ^{1}H NMR spectra (500 MHz, 1,1,2,2-tetrachloroethane-d_2, 50 °C) of poly-**3R** (i) and poly-**4R** (ii). For the signal assignments, see Figures S10 and S11, respectively. (c) Structure of (*P*)-handed helical tubular poly-**4S** with a cylindrical helical cavity. (d) Structures of (*M*)- and (*P*)-handed helical ribbon-like poly-**6R** and poly-**6S** with no helical cavity, respectively. (e) CD and absorption spectra of poly-**3R** (i), poly-**4R** (ii), poly-**3S** (iii), and poly-**4S** (iv) in chloroform at 25 °C. [polymer] = 5.0 × 10^{-5} M. (f) Normalized PL (bottom), CPL (middle), and g_{lum} (top) spectra of poly-**3R** (i), poly-**4R** (ii), poly-**3S** (iii), and poly-**4S** (iv) in chloroform at room temperature. The g_{lum} values are defined as $2(I_L - I_R)/(I_L + I_R)$, where I_L and I_R are the PL intensities of the left- and right-handed circularly polarized light, respectively. λ_{ex} = 300 nm. [polymer] = 5.0 × 10^{-5} M.

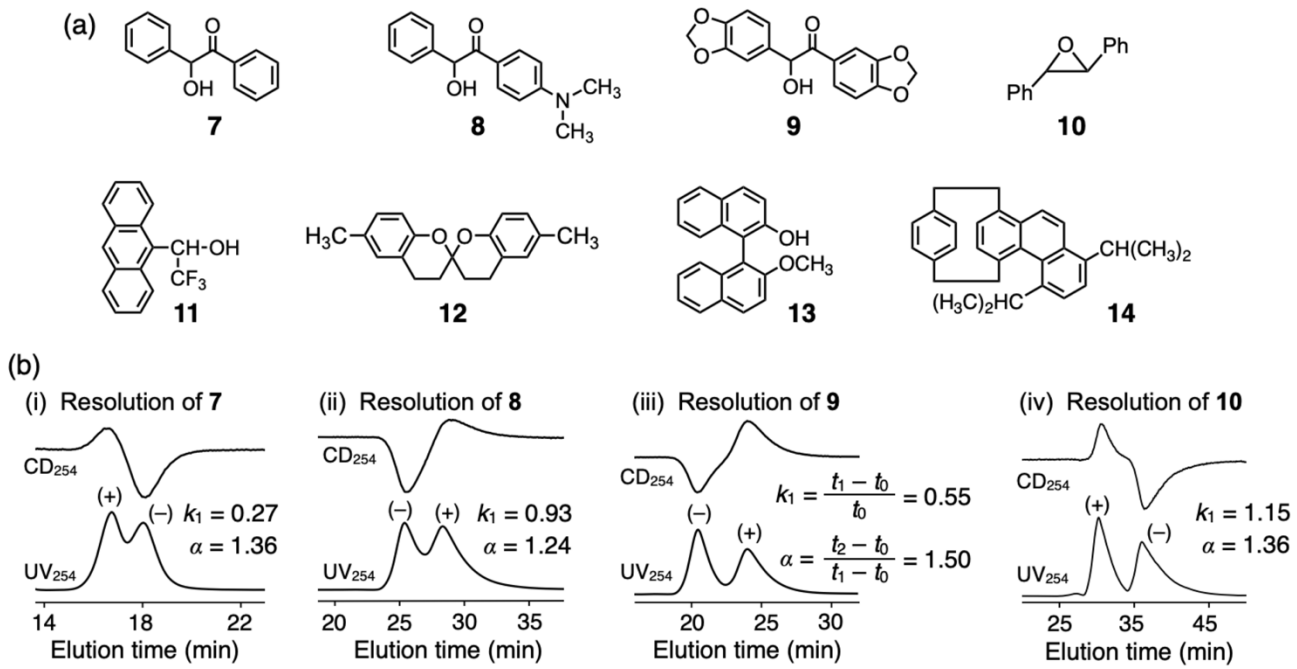

Figure 4. (a) Structures of racemates (**7**–**14**). (b) HPLC chromatograms for the resolutions of **7** (i), **8** (ii), **9** (iii), and **10** (iv) on the poly-**4R**-based CSP at 0°C under reversed-phase conditions. Eluent: methanol/water (95/5, v/v).

Table 2. Resolution results of racemates (**7**–**14**) on CSPs consisting of poly-**3R**, poly-**4R**, poly-**4S**, and poly-**6R** [a]

Racemate	poly-**3R**		poly-**4R**		poly-**4S**		poly-**6R**	
	k_1	α	k_1	α	k_1	α	k_1	α
7[b]	0.02	1.0	0.27	1.36 (+)	0.26	1.31 (–)	0.06	1.0
8[b]	0.04	1.0	0.93	1.24 (–)	0.94	1.23 (+)	0.25	ca.1 (+)
9[b]	0.01	1.0	0.55	1.50 (–)	0.54	1.51 (+)	0.17	1.0
10[b]	0.25	1.0	1.15	1.36 (+)	1.25	1.40 (–)	0.24	1.0
11[c]	0.25	1.0	3.92	1.18 (–)	3.78	1.12 (+)	0.94	1.0
12[d]	0.24	1.0	1.36	1.20 (–)	1.47	1.14 (+)	0.28	1.0
13[e]	0.17	1.0	1.14	1.09 (+)	1.11	1.10 (–)	0.46	1.0
14[f]	0.10	1.0	0.80	1.17 (+)	0.78	1.17 (–)	0.30	1.0

[a] Column: 25 × 0.20 (i.d.) cm. The signs in parentheses represent the Cotton effect signs at 254 nm of the first-eluted enantiomers. [b] Eluent: methanol/water (95/5, v/v); temperature: 0 °C; flow rate: 0.06 mL min^{-1}. [c] Eluent: methanol/water (75/25, v/v); temperature: 20 °C; flow rate: 0.06 mL min^{-1}. [d] Eluent: methanol; temperature: 20 °C; flow rate: 0.10 mL min^{-1}. [e] Eluent: acetonitrile/water (40/60, v/v); temperature: 20 °C; flow rate: 0.04 mL min^{-1}. [f] Eluent: ethanol; temperature: 20 °C; flow rate: 0.06 mL min^{-1}.

positions of the spirobiindane segments of the designer precursor polymers, respectively (Figure 1a,b). In fact, a minimized model structure of poly-**4R** revealed that poly-**4R** has a rigid-rod tightly-twisted (*M*)-handed 4_1 helical tubular ladder structure with a hydrophobic cylindrical helical cavity of ca. 1 nm in diameter (see Figure 5a), while poly-**6R** possesses no helical cavity along the (*M*)-handed extended ribbon-like helical backbone (see Figure 5b). All the hydroxy groups of poly-**4R** are located in the helical groove region, so that the surface of the cylindrical helical cavity is fully covered with the π-conjugated planes of the dibenzo[*a*,*h*]anthracene units (Figure 5a). The rigid-rod robust tubular helical ladder structure of poly-**4R** was further supported by almost no temperature- and solvent-dependent CD and absorption spectra (Figure S15).

Enantioseparation on Tightly-Twisted One-Handed Helical Tubular Ladder Polymers with a π-Electron-Rich Cylindrical Helical Cavity

The π-conjugated planes of the dibenzo[*a*,*h*]anthracene units in the (*M*)-handed helical poly-**4R** backbone are oriented parallel to the main-chain helical axis with an (*M*)-handed helical array. This implies that the tightly-twisted one-handed helical tubular ladder polymers of poly-**4R** and poly-**4S** have the potential for separating enantiomers through π–π and/or hydrophobic interactions within the π-electron-rich hydrophobic helical cavities. We then investigated the chiral recognition abilities of poly-**4R** and poly-**4S** as CSPs for HPLC under reversed-phase conditions (for details of the preparation of the CSPs for HPLC, see Methods). Poly-**4R** and poly-**4S** are highly soluble or swellable in common organic solvents when used as eluents for normal-phase HPLC conditions, such as *n*-hexane/alcohol mixtures. Therefore, their chiral recognition abilities could not be evaluated under normal-phase conditions. The CSPs composed of an optically-active, but random-coil precursor polymer (poly-**3R**) and an (*M*)-handed extended ribbon-like helical ladder polymer with no helical cavity (poly-**6R**) were also prepared for comparison. The resolution results of eight racemates (**7**–**14** in Figure 4a) on these four CSPs evaluated under reversed-phase conditions are summarized in Table 2, in which k_1 and α are the retention and separation factors, respectively, and can be estimated by the following equations; $k_1 = (t_1 - t_0)/ t_0$ and $\alpha = (t_2 - t_0)/ (t_1 - t_0)$, where t_0 is the hold-up time and t_1 and t_2 are the retention times of the first- and second-eluted enantiomers, respectively (see also Figure 4b(iii)).

The one-handed helical tubular ladder polymers of poly-**4R** and poly-**4S** completely or partially separated a variety of aromatic racemates with a point chirality (**7**–**11**) as well as a chiral spiro compound (**12**), an axially chiral biaryl (**13**), and a planar chiral cyclophane (**14**) into enantiomers with opposite enantioselectivities from each other (Table 2), as shown in the typical chromatograms for the resolutions of **7**–**10** using poly-**4R** as a CSP obtained with dual UV and CD detectors (Figure 4b). In sharp contrast, the random-coil precursor polymer (poly-**3R**) and one-handed helical ribbon-like ladder polymer with no helical

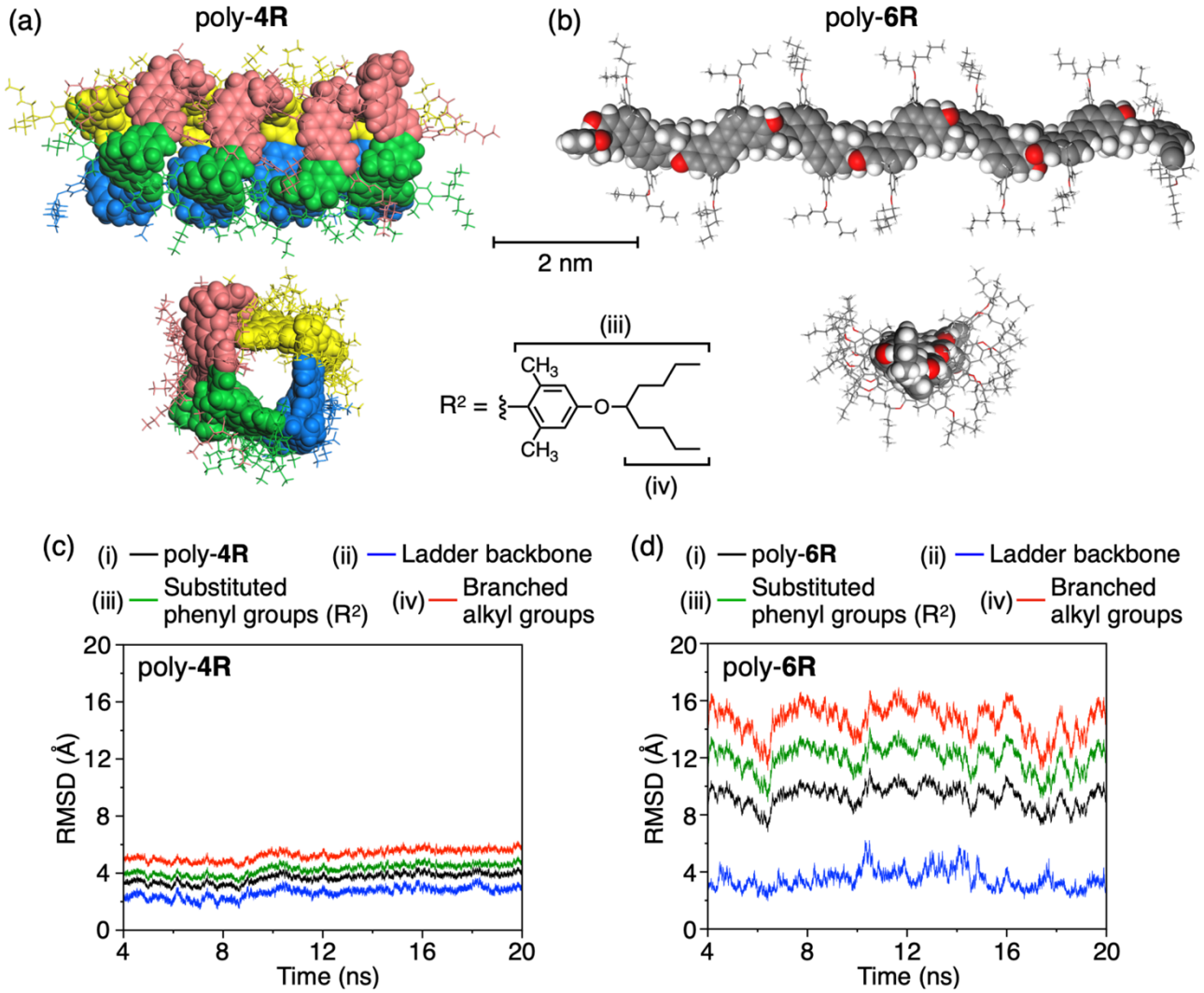

Figure 5. (a,b) The minimized geometries of (*M*)-handed helical tubular poly-**4R** (a) and ribbon-like poly-**6R** (b). (c,d) RMSD plots of whole (i) and partial (ii–iv) structures of poly-**4R** (c) and poly-**6R** (d). The systems seemed to be equilibrated within first 4 ns, and hence the RMSD plots are shown from 4.0 to 20.0 ns.

cavity (poly-**6R**) could not separate all the tested racemates (**7**–**14**) under the same conditions (Table 2). These results definitely indicated the primary role of the tightly-twisted one-handed helical tubular ladder structure with a π-electron-rich hydrophobic helical cavity in the efficient enantioseparations. We presumed that one of the aromatic enantiomers would be favorably encapsulated within the hydrophobic one-handed helical cylindrical cavity in a diastereoselective fashion through attractive π–π and/or hydrophobic interactions, resulting in emergence of the highly-enantioseparation capability under the reversed-phase conditions.

To gain insight into the relationships between the helical structures and chiral recognition abilities, we performed MD simulations of poly-**4R** and poly-**6R** (see Videos S1–3 and S4–6, respectively, and Section 4 in the Supporting Information) and the root-mean-square deviation (RMSD) plots of poly-**4R**, poly-**6R**, and their partial structures are shown in Figure 5c,d. We found that the (*M*)-handed 4_1 helical tubular structure of poly-**4R** is stable and the helical cavity is maintained during the simulation (Figure 5c), whereas their branched alkoxy groups are relatively dynamic (Figure 5c(iv)) and interfere with the accessibility for the guest racemic molecules to the aromatic surfaces outside (Figure S16). One of the branched alkoxy groups occasionally approached the groove region but no deep insertion inside the cavity was observed (Figure S17b). These MD results revealed that the helical cavity of poly-**4R** is mostly free from the branched alkoxy groups that do cover the external aromatic plane of the cavity. Hence, the aromatic racemic molecules could be enantioselectively encapsulated into the π-electron-rich helical cavity of poly-**4R** driven by specific π–π and/or hydrophobic interactions, which was further supported by the molecular mechanics (MM) calculations that the (*M*)-handed 4_1 helical poly-**4R** possesses a sufficiently large helical cavity for encapsulating the chiral molecules (**7**–**14**) and further stabilized by inclusion complex formations (Figure S18 and Table S2).

On the other hand, the (*M*)-handed helical ribbon-like poly-**6R** is more dynamic than poly-**4R** (Figure 5d) and the side chains direct the helical axis outward (Figure S16d). Because both sides of the π-electron-rich aromatic surfaces are free and no interaction between the aromatic planes and side chains are expected, the aromatic surfaces can be exposed to the solvent and/or guest molecules (Figures 5d and S16d). However, the significantly lower k_1 values of the racemates (**7**–**14**) on the ribbon-like helical poly-**6R** as well as the random-coil precursor polymer (poly-**3R**) than those of the tubular helical poly-**4R** and poly-**4S** (Table 2) indicate the primary importance of the π-electron-rich tubular helical cavity formed in the poly-**4R** and poly-**4S**, which dictated the emergence of a high enantioseparation ability. The fact that the k_1 values of the racemates (**7**–**10**) on poly-**4R** tended to increase with an increase in the water content of the eluents, while keeping the α values almost unchanged (Table S3), also supports the inclusion complex formations via π–π and/or hydrophobic interactions between the CSPs and the aromatic racemates that are responsible for the observed high resolution ability of poly-**4R**.

Poly-**4R-C8** synthesized by converting the hydroxy groups at the 1,1´-positions of the spirobiindane segments of poly-**4R** into the octyloxy groups (Figures S4, S19, and S20) totally lost the enantioseparation ability toward **7**–**14** accompanied by a significant decrease in their k_1 values (Table S4). This is because the hydrophobic helical cavity of poly-**4R-C8** was most likely filled with the newly-introduced aliphatic octyl chains and could not serve as a chiral recognition site. This result further supports the proposed chiral separation mechanism based on the enantioselective encapsulation of racemic compounds into the helical cavity of the poly-**4R** and poly-**4S**.

Conclusion

In summary, we have succeeded in the first defect-free synthesis of tightly-twisted one-handed helical tubular ladder polymers with a discrete π-electron-rich cylindrical helical cavity fully covered with the π-conjugated planes oriented parallel to the helical axis by acid-promoted alkyne benzannulations. The (*M*)- and (*P*)-handed helical tubular ladder polymers resolved a wide range of racemic hydrophobic aromatics with point, axial, and planar chiralities when used as CSPs for HPLC under the reversed-phase conditions. In sharp contrast, the random-coil precursor polymer and one-handed helical extended ribbon-like ladder polymer composed of the same homochiral spiro skeleton showed no resolution abilities due to the lack of a helical cavity. Consequently, the π-electron-rich tubular helical cavity robustly constructed in the contracted helical ladder framework through the defect-free helical ladderization plays a key role for chiral recognition, within which one of the aromatic enantiomers can be diastereoselectively encapsulated through π–π and/or hydrophobic interactions. We believe that the synthetic strategy that we have developed will contribute to rationally designing a novel class of helical ladder polymers with a controlled helical geometry including helical sense, helical pitch, and inner helical cavity in a rather predictable way combined with calculations, thus providing unique helical-ladder based chiral materials not only for the chiral separation of specific enantiomers and asymmetric catalysis, but also as chiral optoelectronic materials for chirality sensing that may not be achieved by the already prepared traditional helical polymers. Work toward these goals is currently underway in our laboratory.

Acknowledgements

We thank Professor Makoto Yamashita and Dr. Ryo Nakano (Nagoya University) for their assistance in the X-ray crystallographic analysis of (*R*)-**2**. We also thank Mr. Atsushi Tsuzuki (Nagoya University) for his assistance in the preparation of the chiral columns. This work was supported in part by Grant-in-Aid for Specially Promoted Research (no. 18H05209 (E.Y. and T.I.)), Grant-in-Aid for Scientific Research (B) (no. 21H01984 (T.I.)), and Grant-in-Aid for Postdoctoral Fellowship for Overseas Researchers (no. 20F20335 (W.Z.)) from the Japan Society for the Promotion of Science (JSPS KAKENHI) and JST PRESTO (no. JPMJPR21A1 (T.I.)).

Keywords: alkyne benzannulations • chiral recognition • ladder formation • helical cavities • spiro structures

[1] E. Bertoft, *Agronomy* **2017**, *7*, 56.
[2] Y. Meng, F. Lyu, X. Xu, L. Zhang, *Biomacromolecules* **2020**, *21*, 1653–1677.
[3] a) B. J. G. E. Pieters, M. B. van Eldijk, R. J. M. Nolte, J. Mecinović, *Chem. Soc. Rev.* **2016**, *45*, 24–39; b) C. J. Wilson, A. S. Bommarius, J. A. Champion, Y. O. Chernoff, D. G. Lynn, A. K. Paravastu, C. Liang, M.-C. Hsieh, J. M. Heemstra, *Chem. Rev.* **2018**, *118*, 11519–11574.

[4] a) P. Tomasik, C. H. Schilling, *Adv. Carbohydr. Chem. Biochem.* **1998**, *53*, 345–426; b) J. A. Putseys, L. Lamberts, J. A. Delcour, *J. Cereal Sci.* **2010**, *51*, 238–247; c) M. Numata, S. Shinkai, *Chem. Commun.* **2011**, *47*, 1961–1975; d) B. Alberts, A. Johnson, J. Lewis, D. Morgan, M. Raff, K. Roberts, P. Walter, *Molecular Biology of the Cell, 6th ed., Garland Science*, New York, **2015**; e) J. Kadokawa, *Synlett* **2020**, *31*, 648–656.

[5] a) D. J. Hill, M. J. Mio, R. B. Prince, T. S. Hughes, J. S. Moore, *Chem. Rev.* **2001**, *101*, 3893–4011; b) Y. Ferrand, I. Huc, *Acc. Chem. Res.* **2018**, *51*, 970–977; c) Z. C. Girvin, S. H. Gellman, *J. Am. Chem. Soc.* **2020**, *142*, 17211–17223; d) T. A. Sobiech, Y. Zhong, B. Gong, *Org. Biomol. Chem.* **2022**, *20*, 6962–6978.

[6] E. Yashima, N. Ousaka, D. Taura, K. Shimomura, T. Ikai, K. Maeda, *Chem. Rev.* **2016**, *116*, 13752–13990.

[7] a) T. Kawauchi, J. Kumaki, A. Kitaura, K. Okoshi, H. Kusanagi, K. Kobayashi, T. Sugai, H. Shinohara, E. Yashima, *Angew. Chem., Int. Ed.* **2008**, *47*, 515–519; b) T. Kawauchi, A. Kitaura, J. Kumaki, H. Kusanagi, E. Yashima, *J. Am. Chem. Soc.* **2008**, *130*, 11889–11891.

[8] a) R. B. Prince, S. A. Barnes, J. S. Moore, *J. Am. Chem. Soc.* **2000**, *122*, 2758–2762; b) M. Inouye, M. Waki, H. Abe, *J. Am. Chem. Soc.* **2004**, *126*, 2022–2027; c) J.-L. Hou, X.-B. Shao, G.-J. Chen, Y.-X. Zhou, X.-K. Jiang, Z.-T. Li, *J. Am. Chem. Soc.* **2004**, *126*, 12386–12394; d) J. Garric, J. M. Léger, I. Huc, *Angew. Chem., Int. Ed.* **2005**, *44*, 1954–1958; e) T. Kawauchi, A. Kitaura, M. Kawauchi, T. Takeichi, J. Kumaki, H. Iida, E. Yashima, *J. Am. Chem. Soc.* **2010**, *132*, 12191–12193; f) N. Chandramouli, Y. Ferrand, G. Lautrette, B. Kauffmann, C. D. Mackereth, M. Laguerre, D. Dubreuil, I. Huc, *Nat. Chem.* **2015**, *7*, 334–341; g) N. Ousaka, F. Mamiya, Y. Iwata, K. Nishimura, E. Yashima, *Angew. Chem., Int. Ed.* **2017**, *56*, 791–795; h) T. Ikai, S. Kawabata, F. Mamiya, D. Taura, N. Ousaka, E. Yashima, *J. Am. Chem. Soc.* **2020**, *142*, 21913–21925.

[9] a) N. Ousaka, T. Yamaguchi, E. Yashima, *Chem. Lett.* **2014**, *43*, 512–514; b) T. Ikai, T. Yoshida, *Org. Biomol. Chem.* **2019**, *17*, 8537–8540.

[10] R. L. Van Deusen, *J. Polym. Sci., Part B: Polym. Lett.* **1966**, *4*, 211–214.

[11] a) Y. C. Teo, H. W. H. Lai, Y. Xia, *Chem. - Eur. J.* **2017**, *23*, 14101–14112; b) X. Y. Wang, A. Narita, K. Müllen, *Nat. Rev. Chem.* **2018**, *2*, 0100; c) A. Jolly, D. D. Miao, M. Daigle, J. F. Morin, *Angew. Chem., Int. Ed.* **2020**, *59*, 4624–4633; d) S. Che, L. Fang, *Chem* **2020**, *6*, 2558–2590; e) S. H. Liu, D. B. Xia, M. Baumgarten, *Chempluschem* **2021**, *86*, 36–48.

[12] T. Ikai, T. Yoshida, K. Shinohara, T. Taniguchi, Y. Wada, T. M. Swager, *J. Am. Chem. Soc.* **2019**, *141*, 4696–4703.

[13] a) M. B. Goldfinger, T. M. Swager, *J. Am. Chem. Soc.* **1994**, *116*, 7895–7896; b) M. B. Goldfinger, K. B. Crawford, T. M. Swager, *J. Am. Chem. Soc.* **1997**, *119*, 4578–4593.

[14] M. B. Goldfinger, K. B. Crawford, T. M. Swager, *J. Org. Chem.* **1998**, *63*, 1676–1686.

[15] a) T. Ikai, S. Yamakawa, N. Suzuki, E. Yashima, *Chem. - Asian J.* **2021**, *16*, 769–774; b) W. Zheng, T. Ikai, E. Yashima, *Angew. Chem., Int. Ed.* **2021**, *60*, 11294–11299.

[16] W. Zheng, T. Ikai, K. Oki, E. Yashima, *Nat. Sci.* **2022**, *2*, e20210047.

[17] Z. Yi, H. Okuda, Y. Koyama, R. Seto, S. Uchida, H. Sogawa, S. Kuwata, T. Takata, *Chem. Commun.* **2015**, *51*, 10423–10426.

[18] R. Ammenhäuser, P. Klein, E. Schmid, S. Streicher, J. Vogelsang, C. W. Lehmann, J. M. Lupton, S. C. J. Meskers, U. Scherf, *Angew. Chem., Int. Ed.* **2022**, *61*, e202211946.